energies

Article

Thermodynamic Assessment and Multi-Objective Optimization of Performance of Irreversible Dual-Miller Cycle

Shahriyar Abedinnezhad [1], Mohammad Hossein Ahmadi [2], Seyed Mohsen Pourkiaei [3], Fathollah Pourfayaz [3], Amir Mosavi [4,5,6], Michel Feidt [7] and Shahaboddin Shamshirband [8,9,*]

1 Department of Aerospace Engineering, Sharif University of Technology, Tehran, Iran; sh.abedinnejad@gmail.com
2 Faculty of Mechanical Engineering, Shahrood University of Technology, Shahrood, Iran; mohammadhosein.ahmadi@gmail.com
3 Department of Renewable Energy and Environmental Engineering, University of Tehran, Tehran, Iran; s.mohsenpourkiaei@gmail.com (S.M.P.); pourfayaz@ut.ac.ir (F.P.)
4 Kalman Kando Faculty of Electrical Engineering, Obuda University, 1034 Budapest, Hungary; amir.mosavi@kvk.uni-obuda.hu
5 School of the Built Environment, Oxford Brookes University, Oxford OX30BP, UK
6 Faculty of Health, Queensland University of Technology, Brisbane, QLD 4059, Australia
7 University of Lorraine, LEMTA, 2 avenue de la forêt de Haye 54516 Vandoeuvre les Nancy, France; michel.feidt@univ-lorraine.fr
8 Department for Management of Science and Technology Development, Ton Duc Thang University, Ho Chi Minh City, Vietnam
9 Faculty of Information Technology, Ton Duc Thang University, Ho Chi Minh City, Vietnam
* Correspondence: shahaboddin.shamshirband@tdtu.edu.vn

Received: 17 September 2019; Accepted: 18 October 2019; Published: 21 October 2019

Abstract: In this study, a new series of assessments and evaluations of the Dual-Miller cycle is performed. Furthermore, the specified output power and the thermal performance associated with the engine are determined. Besides, multi-objective optimization of thermal efficiency, ecological coefficient of performance (ECOP) and ecological function (E_{un}) by means of NSGA-II technique and thermodynamic analysis are presented. The Pareto optimal frontier obtaining the best optimum solution is identified by fuzzy Bellman-Zadeh, Linear Programming Technique for Multidimensional Analysis of Preference (LINMAP), and Technique for Order of Preference by Similarity to Ideal Solution (TOPSIS) decision-making techniques. Based on the results, performances of dual-Miller cycles and their optimization are improved. For the results of the condition that ($n < k$) the best point has been LINMAP answer. The thermal efficiency for this point has been 0.5388. In addition, ECOP and E_{un} have been 1.6899 and 279.221, respectively. For the results of the condition that ($n > k$) the best point has been LINMAP and TOPSIS answer. The thermal efficiency for this point has been 0.5385. Also, ECOP and E_{un} have been 1.6875 and 279.7315, respectively. Furthermore, the errors are examined through comparison of the average and maximum errors of the two scenarios.

Keywords: Dual-Miller cycle; thermodynamic analysis; power; ecological coefficient of performance; thermal efficiency; energy; entropy generation; multi-objective optimization (MOO); multi-criteria decision making (MCDM); soft computing; genetic algorithm; finite-time thermoeconomic (FTT)

1. Introduction

There are different approaches applied to evaluate the energy systems [1–4]. Finite-time thermoeconomic (FTT) optimization is among the most appropriate approaches applicable for evaluating the operation quality of internal combustion engine cycles (ICEC) [5–13]. In recent studies of thermodynamic systems [14–23], comprehensive investigations have been carried out [24]. Entropy optimization [25–29], E_{un} criterion [30–34], and ecological coefficient of performance (ECOP) criterion [35–40] are some of the recent various optimization objectives in ICEC analysis. Generally, entropy reduction is not equal to enhancing thermal efficiency or maximum power generation. Under certain circumstances, minimizing entropy generation leads to the highest power generation [41]. Blank et al. [42] investigated the efficiency of an endoreversible air standard dual cycle considering the system heat loss. Chen and colleagues [43] investigated the air standard dual cycle considering the friction and heat loss. Ust and colleagues [44] studied the performance optimization of an irreversible air standard dual cycle taking the impact of internal irreversibility and heat loss into account. Ghatak et al. [45] investigated the efficiency of an endoreversible air standard dual cycle considering the fluid thermal characteristics. Wang et al. [46] carried out a performance analysis considering the finite-time element and internal loss. Ge and colleagues [47] ran a thermodynamic analysis of the irreversible air standard dual cycle. In the thermodynamic assessment and optimization of air standard Miller cycles, Al-Sarkhi and colleagues [48] optimized the power density of a reversible cycle. Chen and colleagues [49,50] assessed the efficiency of an irreversible air standard Miller cycle considering the thermal properties of the working fluid and friction and heat loss of the system. Lin and colleagues [51] conducted an optimization for an irreversible air standard Miller system. Due to the thermodynamic evaluation of single cycles, Gonca et al. and other researchers [52–58] and Gonca [59] analyzed irreversible Dual-Miller cycles taking power and thermal efficiency into account. Ust and colleagues [60] conducted an exergy optimization for an irreversible Dual-Miller cycle. Gonca and colleagues [61,62] analyzed the ECOP of an irreversible Dual-Miller cycle. Wu and colleagues [63,64] investigated the efficiency of an irreversible Dual-Miller cycle considering linear [63] and nonlinear [64] thermal properties of working fluid. Huleihil et al. [65] presented and evaluated a reversible air-standard Otto model through polytropic processes. Gong and colleagues [66] performed a performance optimization of an endoreversible Lenoir cycle, considering heat losses and polytropic processes. Also, Xiong and colleagues [67] conducted a performance optimization of an endoreversible air standard Otto cycle considering heat losses and polytropic processes. Zhang and colleagues [68] designed and evaluated an irreversible universal cycle model, considering heat and friction losses, polytropic stages, and thermal properties of the working fluid.

Multi-objective optimization (MOO) is a valuable method to model various real-life problems simultaneously [69–71]. Answering a multi-objective optimization question needs simultaneous substantiation of various objectives. Consequently, evolutionary algorithms presented and advanced to answer multi-objective problems applying various methods [72]. A proper approach to find a solution to for a multi-objective problem is to examine a group of routes, each satisfies the objectives at an acceptable level and do not interfere with other routes [73]. MOO problems generally represent a practicably numerous collection of routes named frontier of Pareto, which examined vectors that show the possible primary connections in the whole area of the objective function. New studies indicate that MOOs for different energy systems applied in various engineering problems [74–109].

In this study, the performance of the Irreversible Dual-Miller Cycle is studied. Besides, the effect of critical parameters on the performance of the Dual-Miller cycle is investigated. Key parameters that presented include ε, ρ and the n. The effects of these parameters on the power, efficiency, ECOP, and E_{un} of the system are evaluated. Then and MOO calculation is performed to obtain the best point of performance of the Dual-Miller Cycle.

2. Dual-Miller Cycle through a Polytropic Stage

In order to accurately model the operation of energy systems, it is necessary to consider all of the factors influencing their performance [110–112]. Figure 1 represents the diagram of an air standard Dual-Miller cycle. To increase the accuracy of performance assessment, the polytropic process replaces by the reversible adiabatic stage, which is impractical to attain in the improved Dual-Miller cycle [64]. As depicted in Figure 1, cycle 1–2–3–4–5–6–1 represents the condition in which $n = k$. In the Dual-Miller cycle, the basic concept is the same as the Atkinson cycle in which the intake valves are kept open in part of the compression process. However, in Miller cycles, heat rejection is more. Consequently, the intake process can be replaced with a two-step heat rejection process: step one fresh air admittance as a constant volume process and step two partial compression while the valves are still open as a constant pressure compression. The combustion process is as well a two-step process in which the ignition first rises the pressure, then expansion begins with valves partially open, then the valves will be closed up to the end of the complete expansion. The process 1-2 is a reversible compression process corresponding to 1′-2 that is the irreversible compression. Heat addition occurs in two steps: processes 2-3 and 3-4 reversible or 3-4′ irreversible that lead to higher pressure and temperature. Exhaust process or expansion occurs in 4-5 or 4′-5. The intake process is replaced by a two-step heat rejection that can be seen in processes 5-6 and 6-1 or 6-1′. As can be seen in the figure, for each value of n a different actual compression/expansion process is defined. For $n < k$ the endpoint of compression and expansion 2 and 5 are taken as the common final point between isentropic and actual process and the beginning point 1′ and 4′ vary between the two processes conversely for $n > k$ the beginning points of each process are the common references and the endpoints vary in ideal and actual processes. In both cases, the effective area encompassed by the whole process for the actual cycle must be less than the ideal cycle, and this is the reason why $\Delta s < 0$ can be seen in both cases that don't violate second law at all.

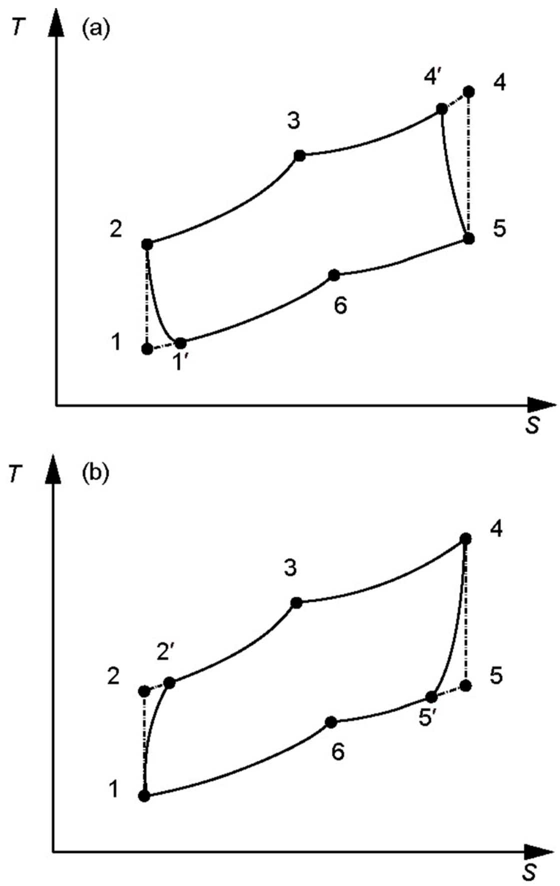

Figure 1. *T*-*S* diagram of Dual-Miller cycle (DMC): n less than the k (**a**) and n higher than the k (**b**) [102].

2.1. Ideal Air Standard Dual-Miller Cycle

In ideal gas systems (n equal to k), the state elements of each stage can be practically obtained, by the ideal gas state equation. According to the first law of thermodynamics, the heat transfer rates and power generation of the cycle can be determined. Equation (1) presents ε, λ, ρ, and r_M, respectively:

$$\varepsilon = \frac{V_1}{V_2},\ \lambda = \frac{P_3}{P_2},\ \rho = \frac{V_4}{V_3},\ r_M = \frac{V_6}{V_1} \tag{1}$$

The primary thermodynamic equations of each stage defined as:

$$T_2 = T_1 \varepsilon^{k-1} \tag{2}$$

$$T_3 = T_2 \lambda \tag{3}$$

$$T_4 = T_3 \rho \tag{4}$$

$$T_5 = T_4 \left(\frac{\rho}{\varepsilon \cdot r_M} \right)^{k-1} \tag{5}$$

$$T_6 = T_5 \left(\frac{r_M^k}{\lambda \cdot \rho^k} \right) \tag{6}$$

$$T_1 = \frac{T_6}{r_M} \tag{7}$$

The total heat absorption and heat rejection are as follows:

$$Q_{in} = Q_{23} + Q_{34} = \dot{m}\Big(C_v (T_3 - T_2) + C_p (T_4 - T_3) \Big) \tag{8}$$

$$Q_{out} = Q_{56} + Q_{61} = \dot{m}\Big(C_v (T_5 - T_6) + C_p (T_6 - T_1) \Big) \tag{9}$$

A desirable reversible air standard Dual-Miller cycle, the heat transfer impact is not considered, while it considered for an actual DMC. This waste is considered relevant to the temperature difference of the cylinder wall and the functioning fluid as follows [102,103]

$$Q_l = \frac{B}{2}(T_2 + T_4 - 2T_0) \tag{10}$$

B is the heat transfer coefficient, and T_0 is ambient temperature. The power production and performance are calculated as:

$$P = Q_{in} - Q_{out} \tag{11}$$

$$\eta = \frac{P}{Q_{in} + Q_l} \tag{12}$$

2.2. Air Standard Dual-Miller Cycle ($n < k$)

As it is depicted in Figure 1, T_1 in a Dual-Miller cycle (n less than the k) is higher than the T_1 in the air standard Dual-Miller cycle. In order to keep T_2 fixed through the compression stage, heat is extracted through the polytropic stage 1′–2. Considering heat waste through the heat input stage, $T_{4'}$ is lower than T_4. In order to keep T_5 fixed, heat should be increased through the polytropic stage 4′–5.

The equations of each stage are defined as:

$$T_2 = T_{1'}\varepsilon^{(\frac{k(n-1)}{n})} \tag{13}$$

$$T_5 = T_{4'}\left(\frac{\rho}{\varepsilon \cdot r_M}\right)^{\frac{k(n-1)}{n}} \tag{14}$$

The heat transfer rate of polytropic stage 1′–2, is defined as follows:

$$Q_{1'2} = \dot{m}C_v\left(\frac{k-n}{n-1})(T_2 - T_{1'}\right) \tag{15}$$

The heat transfer rate of stages 2–3 and 3–4′, are defined as follows:

$$Q_{23} = \dot{m}C_v(T_3 - T_2) \tag{16}$$

$$Q_{34'} = \dot{m}C_p(T_{4'} - T_3) \tag{17}$$

The heat transfer rate of stage 4′–5, is defined as follows:

$$Q_{4'5} = \dot{m}C_v\left(\frac{k-n}{n-1})(T_{4'} - T_5\right) \tag{18}$$

The heat transfer rate of stages 5–6 and 6–1′, are defined as follows:

$$Q_{56} = \dot{m}C_v(T_5 - T_6) \tag{19}$$

$$Q_{61'} = \dot{m}C_p(T_6 - T_{1'}) \tag{20}$$

The heat input of the cycle is

$$Q_{in1} = Q_{23} + Q_{34'} + Q_{4'5} \tag{21}$$

The heat output of the cycle is

$$Q_{out1} = Q_{1'2} + Q_{56} + Q_{61'} \tag{22}$$

In a desirable air standard Dual-Miller cycle, the ratio of the highest temperature to the lowest temperature is defined as follows:

$$\frac{T_4}{T_1} = \rho \cdot \lambda \cdot \varepsilon^{k-1} \tag{23}$$

As stated by [102,103,109], the heat waste ratio is defined as follows:

$$Q_{l1} = \frac{B}{2}(T_2 + T_{4'} - 2T_0) \tag{24}$$

As a result, the generated power and the first law efficiency of the system are defined as follows:

$$P_1 = Q_{in1} - Q_{out1} \tag{25}$$

$$\eta_1 = \frac{P_1}{Q_{in}} = \frac{P_1}{Q_{23} + Q_{34'} + Q_{4'5} + Q_{l1}} \tag{26}$$

Considering the assumption in [104], the exhaust gas recirculation due to the heat transfer loss is determined as follows:

$$\sigma_{q1} = \frac{B(T_2 + T_{4'} - 2T_0)}{2T_0} \tag{27}$$

The exhaust gas recirculation due to the working fluid heat rejection is defined as [105]:

$$\sigma_{pq1} = m\left(\int_{T_{1'}}^{T_6} C_p\left(\frac{1}{T_0} - \frac{1}{T}\right)dT + \int_{T_6}^{T_5} C_v\left(\frac{1}{T_0} - \frac{1}{T}\right)dT + \int_{T_{1'}}^{T_2} C_v\left(\frac{k-n}{n-1}\right)\left(\frac{1}{T_0} - \frac{1}{T}\right)dT\right) \tag{28}$$

As a result, the total entropy generation (σ_{un1}) of the system is defined as follows:

$$\sigma_{un1} = \sigma_{q1} + \sigma_{pq1} \tag{29}$$

According to refs. [30–34], ECOP of the cycle is defined as follows:

$$\mathrm{ECOP} = \frac{P_1}{T_0\sigma_{un1}} \tag{30}$$

According to references [30–34], E_{un} is defined as follows:

$$E_{un1} = P_1 - T_0\sigma_{un1} \tag{31}$$

2.3. Air Standard Dual-Miller Cycle ($n > k$)

As depicted in Figure 2, T_2 the highest temperature of the adiabatic stage 1–2 is less than that of the polytropic stage, due to the heat waste through the isochoric stage 2–3 (n higher than the k). Thus, more heat applied through the polytropic stage 1–2′. On the other hand, heat is extracted through the stage 4–5′ as T_5 the minimum temperature of the adiabatic stage 4–5 is greater than that of the polytropic stage 4–5′ taking the heat waste through the isobaric stage 3–4, into account.

The equations of polytropic stages are defined as follows:

$$T_{2'} = T_1 \cdot \varepsilon^{n-1} \tag{32}$$

$$T_{5'} = T_4 \cdot \left(\frac{\rho}{\varepsilon \cdot r_M}\right)^{n-1} \tag{33}$$

For polytropic stage 1–2′, the heat transfer ratio is defined as:

$$Q_{12'} = \dot{m}C_v\left(\frac{n-k}{n-1}\right)(T_{2'} - T_1) \tag{34}$$

For stages 2′–3 and 3–4, heat transfer rates are defined as:

$$Q_{2'3} = \dot{m}C_v(T_3 - T_{2'}) \tag{35}$$

$$Q_{34} = \dot{m}C_p(T_4 - T_3) \tag{36}$$

For stage 4–5′, the heat transfer rate is defined as:

$$Q_{45'} = \dot{m}C_v\left(\frac{n-k}{n-1}\right)(T_4 - T_{5'}) \tag{37}$$

For stages 5′–6 and 6–1′, heat transfer rates are defined as:

$$Q_{5'6} = \dot{m}C_v(T_{5'} - T_6) \tag{38}$$

$$Q_{61} = \dot{m}C_p(T_6 - T_1) \tag{39}$$

The net heat input ratio is calculated as:

$$Q_{in2} = Q_{12'} + Q_{2'3} + Q_{34} \tag{40}$$

The net heat output ratio is calculated as:

$$Q_{out2} = Q_{45'} + Q_{5'6} + Q_{61} \tag{41}$$

The heat waste ratio is calculated as [102,103]:

$$Q_{l2} = \frac{B}{2}(T_{2'} + T_4 - 2T_0) \tag{42}$$

The power generation and the first law efficiency of the system are defined as follows:

$$P_2 = Q_{in2} - Q_{out2} \tag{43}$$

$$\eta_2 = \frac{P_2}{Q_{in}} = \frac{P_2}{Q_{12'} + Q_{2'3} + Q_{34} + Q_{l2}} \tag{44}$$

The exhaust gas recirculation of the heat transfer loss is calculated as follows [104]:

$$\sigma_{q2} = \frac{B(T_{2'} + T_4 - 2T_0)}{2T_0} \tag{45}$$

The exhaust gas recirculation based on the functioning fluid heat rejection is as follows [105]:

$$\sigma_{pq2} = m\left(\int_{T_{1'}}^{T_6} C_p\left(\frac{1}{T_0} - \frac{1}{T}\right)dT + \int_{T_6}^{T_{5'}} C_v\left(\frac{1}{T_0} - \frac{1}{T}\right)dT + \int_{T_E}^{T_4} C_v\left(\frac{n-k}{n-1}\right)\left(\frac{1}{T_0} - \frac{1}{T}\right)dT\right) \tag{46}$$

The total exhaust gas recirculation of the system is defined as follows:

$$\sigma_{un2} = \sigma_{q2} + \sigma_{pq2} \tag{47}$$

According to refs. [30–34], ECOP of the cycle is defined as follows:

$$\mathrm{ECOP} = \frac{P_2}{T_0\sigma_{un2}} \tag{48}$$

The E_{un} is defined as follows:

$$E_{un2} = P_2 - T_0\sigma_{un2} \tag{49}$$

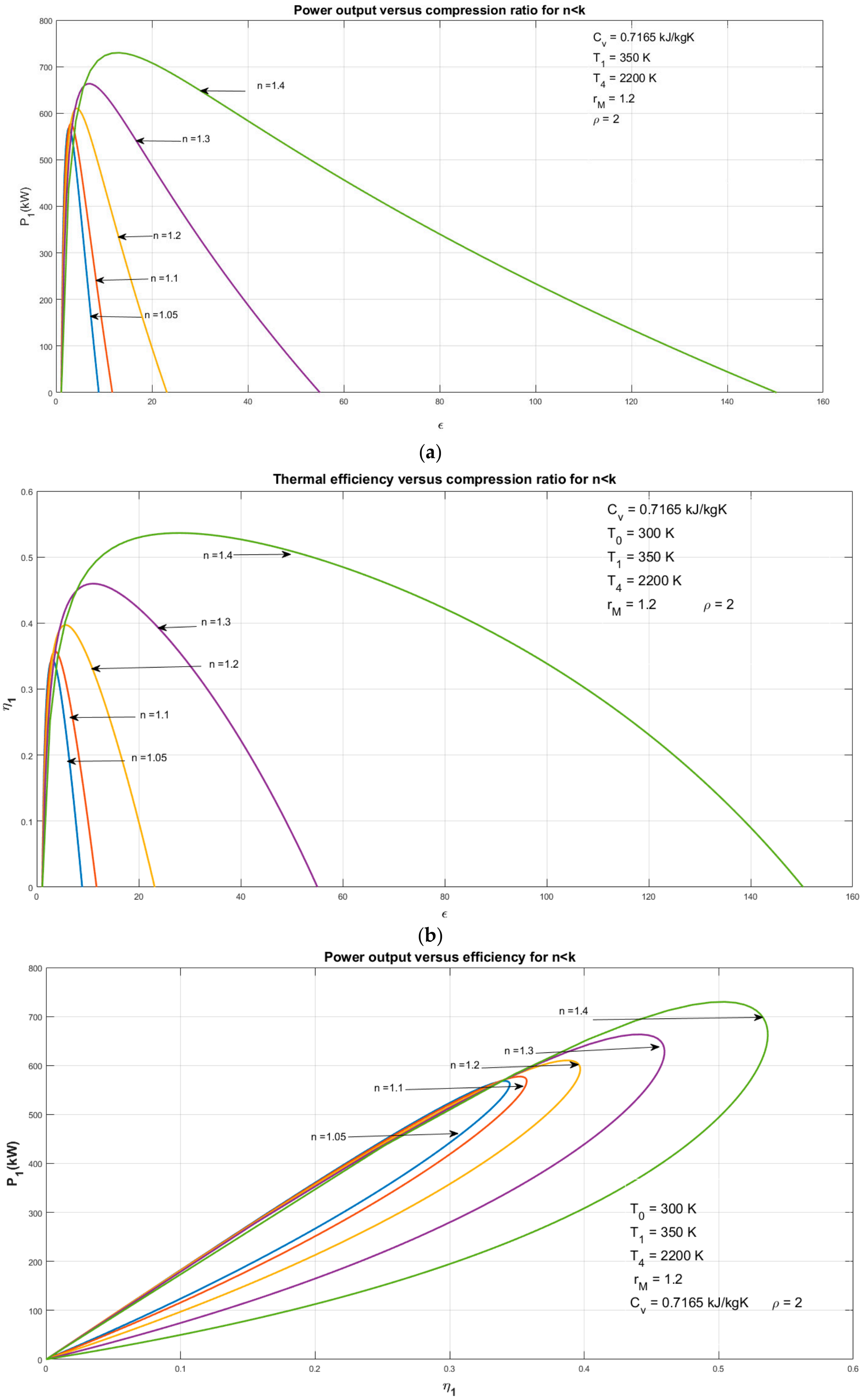

(**a**)

(**b**)

(**c**)

Figure 2. Impact of n ($n < k$) on P_1–ε (**a**), η_1–ε (**b**) and P_1–η_1 (**c**) relations.

3. Optimization Development: Evolutionary Algorithm

Genetic Algorithm

Genetic algorithms provide the best suitable answer of the studding system employing a repetitious and random exploration approach and duplicate it by simple basics of biological evolution [72]. The individual that is a possible solution to the optimization case [73] presents the values of the decision elements. More explanations about Genetic algorithms and its function is available in References [72,73].

4. Results and Discussions

4.1. Performance Analyses for the Condition n Less than the k

Figure 2 depicts the impact of n on the performance relations among power, efficiency and compression ratio. It is evident that as ε increases, P_1 and η_1 initially increase and finally decrease. It should be noted that that $P_{1,\max}$ and $\eta_{1,\max}$ do not take place at the same time. On the other hand, $P_{1,\max}$ and $\eta_{1,\max}$ increase by the enhancement of n. Furthermore, the efficiency at maximum power rises by the enhancement of n.

Figure 3 illustrates the impact of ρ on the relationship between P_1 and ε at n = 1.2. As depicted in Figure 3, the output power has an early rise to the pick, and gradually falls at the various values of the compression ratio (ε) and the cut-off ratio (ϱ). However, at the constant value of the compression ratio (ε), as the value of the cut-off ratio (ϱ) rises the output power also follows the rise.

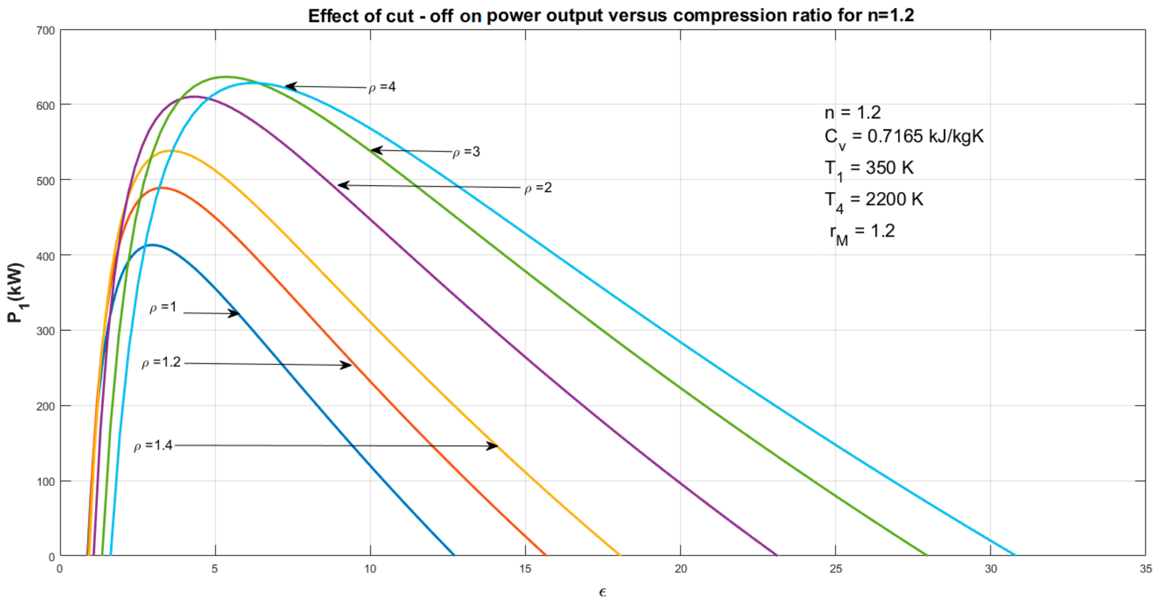

Figure 3. Effect of ρ on P_1 versus ε (n = 1.2).

Figure 4 depicts the E_{un} changes against P_1 and η_1 relations at various n. It is obvious that n has a direct relationship with P_1 and η_1. The maximum E_{un} point is adjacent to $P_{1,\max}$ and $\eta_{1,\max}$. In other words, the optimum values of P_1 and η_1 could be achieved when E_{un} is optimized.

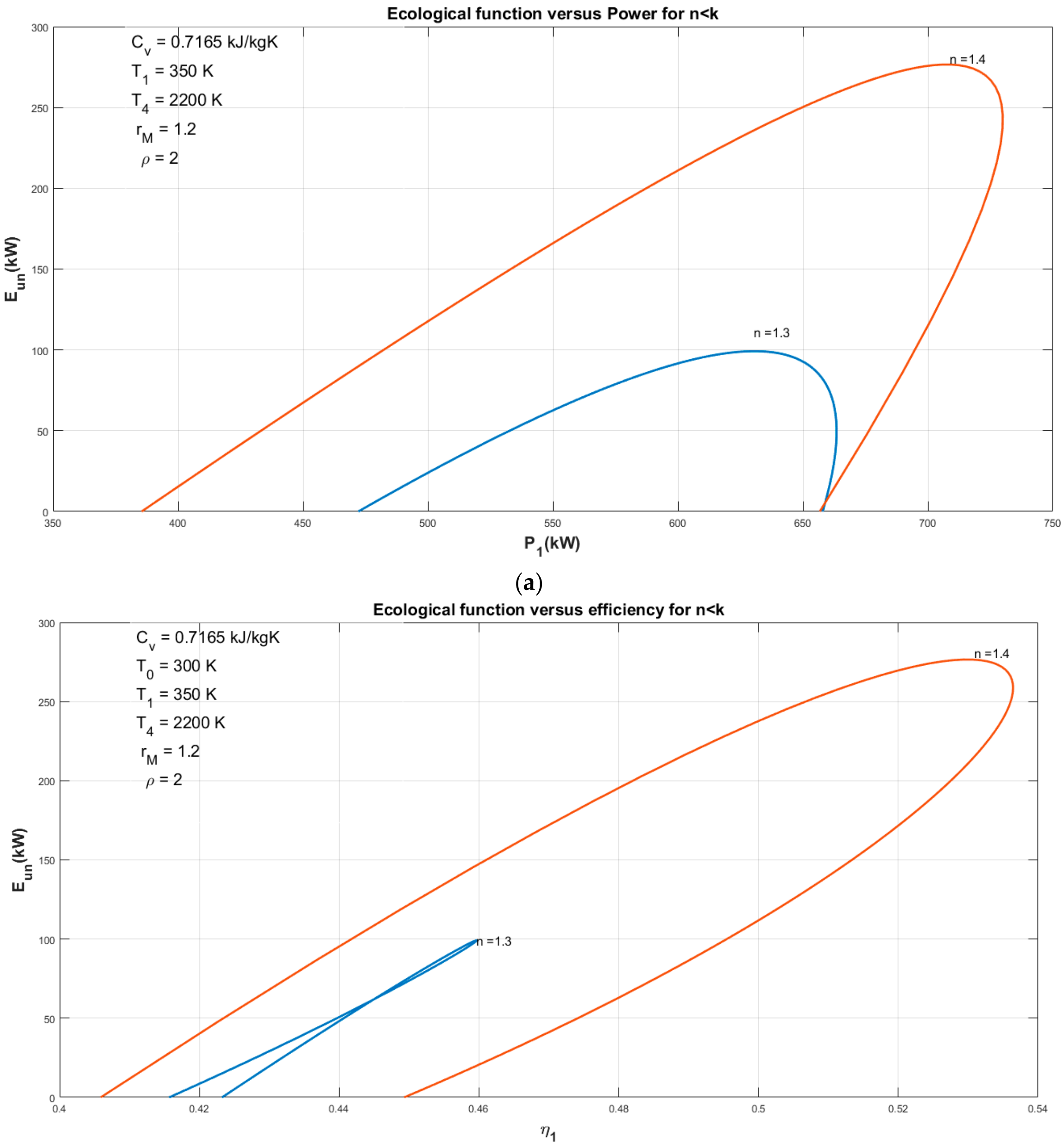

(**a**)

(**b**)

Figure 4. Impact of ($n < k$) n on E_{un}–P_1 (**a**) and E_{un}–η_1 (**b**).

As shown in Figure 5a. As the compression ratio increases, with a very steep gradient, ECOP first increases to its maximum point and then begins to decrease. Also, in a constant compression, the ECOP increases with the increase of the n ($n < k$). Figure 5b,c shows that the maximum value of the coefficient of performance for various n ($n < k$) will occur at almost the maximum power and maximum thermal efficiency.

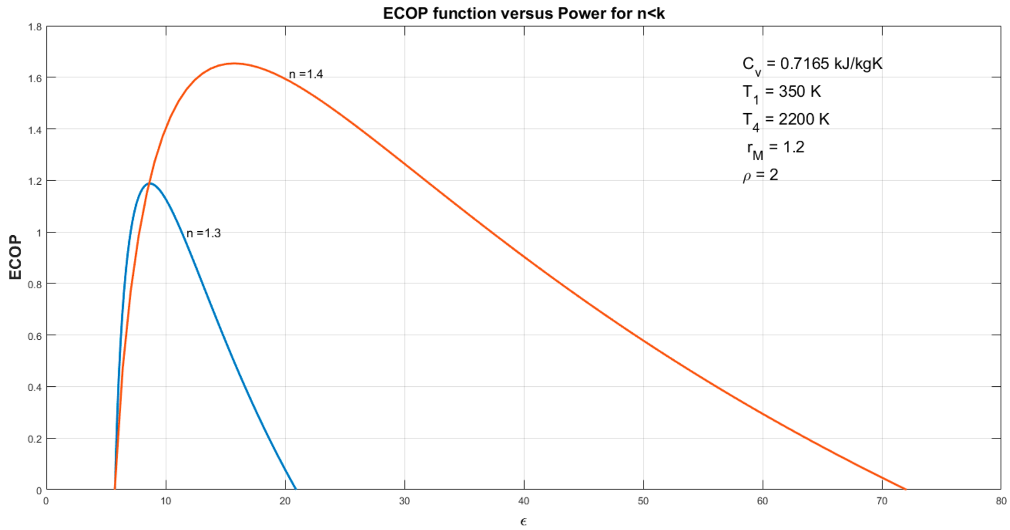

(**a**)

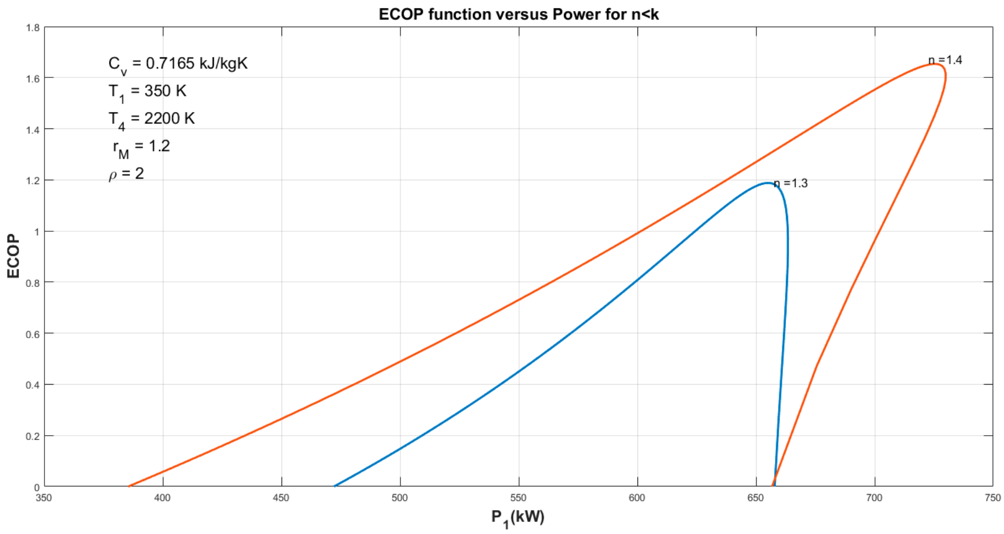

(**b**)

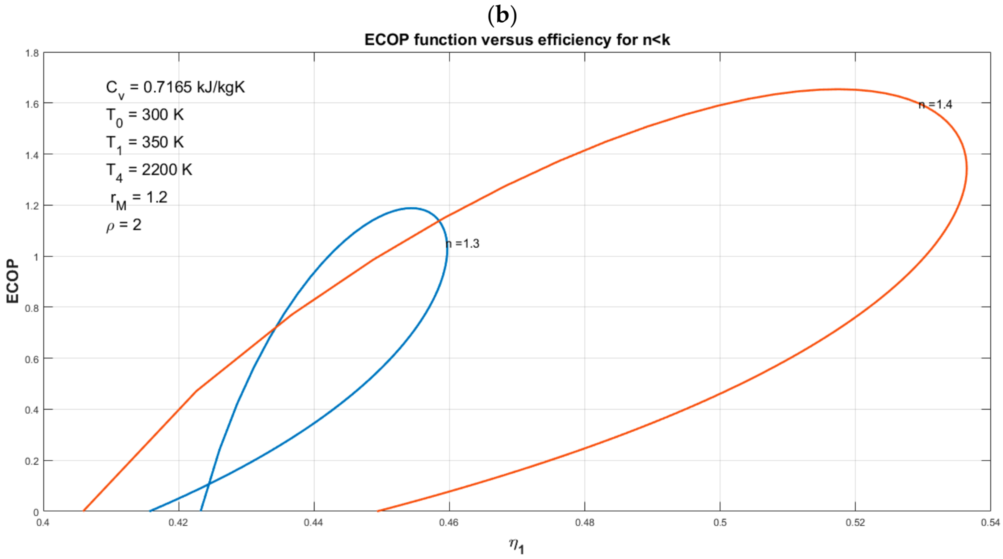

(**c**)

Figure 5. Impact of n ($n < k$) on ecological coefficient of performance (ECOP)–ε (**a**), ECOP–P_1 (**b**) and ECOP–η_1 (**c**).

4.2. Performance Evaluation at the Condition of n higher than the k

Figure 6 depicts the impact of n on the performance relations among power, efficiency and compression ratio. It is obvious that when ε increases, P_2 and η_2 initially increase and finally decrease. Enhancing n leads to a slow reduction of P_2 and η_2. It should be noted that $P_{2,\,max}$ and $\eta_{2,\,max}$, do not take place at the same value of epsilon. Hence, the η_2 at $P_{2,\,max}$ reduces by enhancement of n.

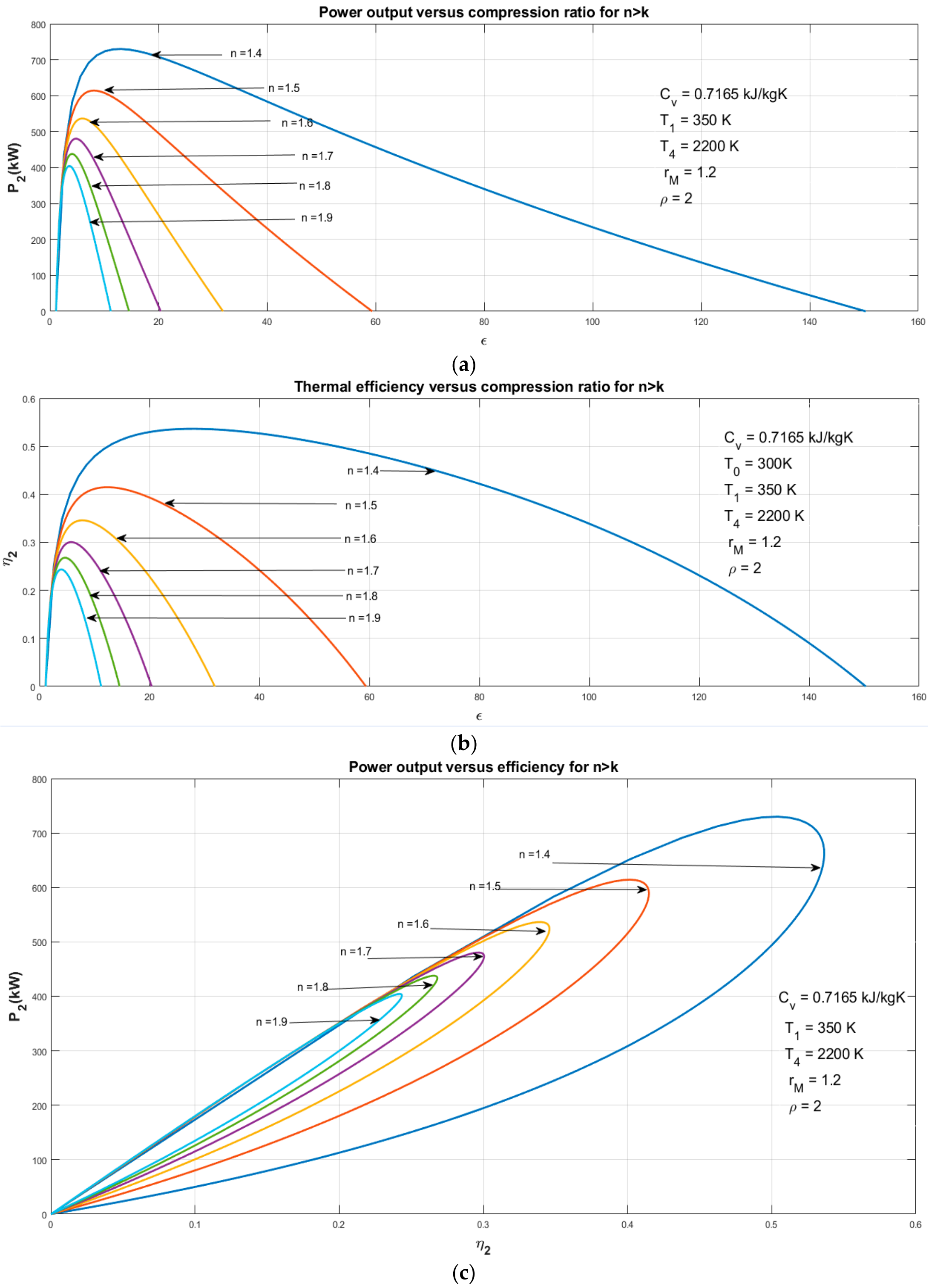

Figure 6. Impact of n ($n > k$) on P_2–ε (**a**), η_2–ε (**b**) and P_2–η_2 (**c**).

Figure 7 illustrates the impact of ρ on the relationship between P_2 and ε at $n = 1.6$. As depicted in Figure 7, the output power at the beginning rises to its maximum then gradually decreases as the compression ratio (ε) rises at the various cut-off ratio (ϱ). However, at the constant compression ratio (ε), when the cut-off ratio (ϱ) rises the value of the output power declines.

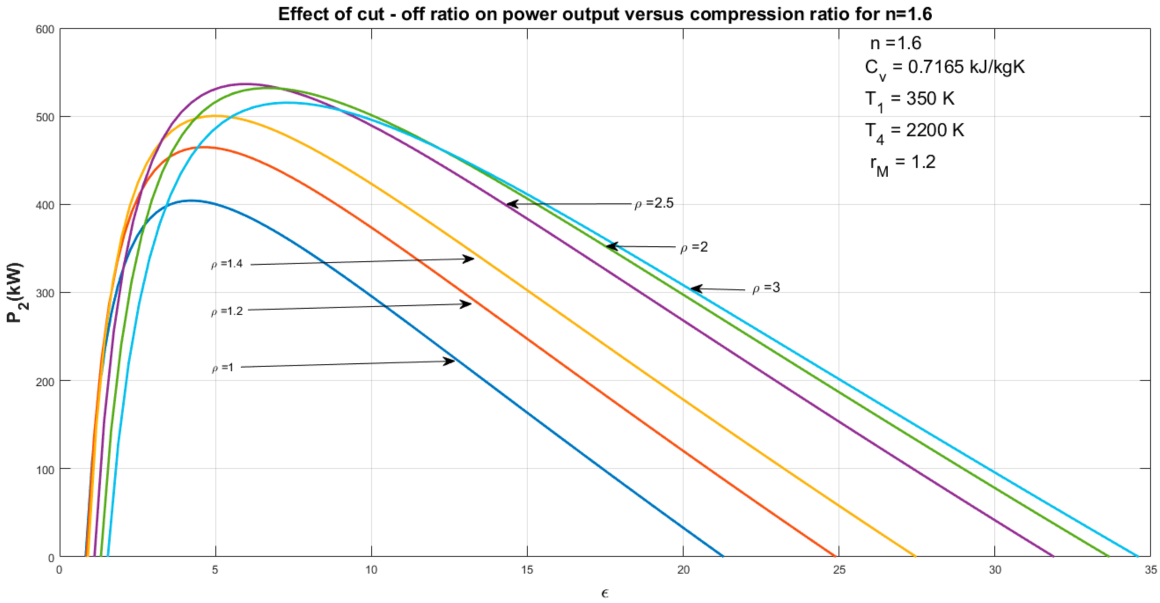

Figure 7. Effect of ρ on P_2 against ε ($n = 1.6$).

Figure 8 presents the E_{un} impact on P_2 and η_2 at various n. It is obvious that increasing n leads to E_{un}, and E_{un} reduction. The $E_{un,\max}$ is adjacent to $P_{2,\max}$ and $\eta_{2,\max}$. In other words, othe ptimum values of P_2 and η_2 could be achieved when E_{un} is optimized.

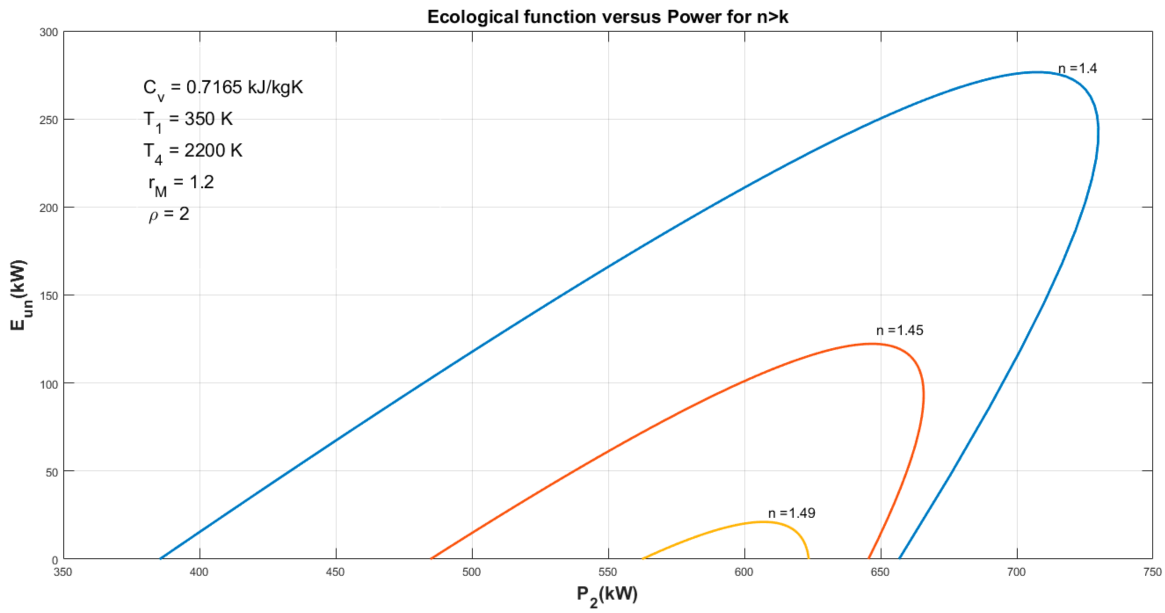

(**a**)

Figure 8. *Cont.*

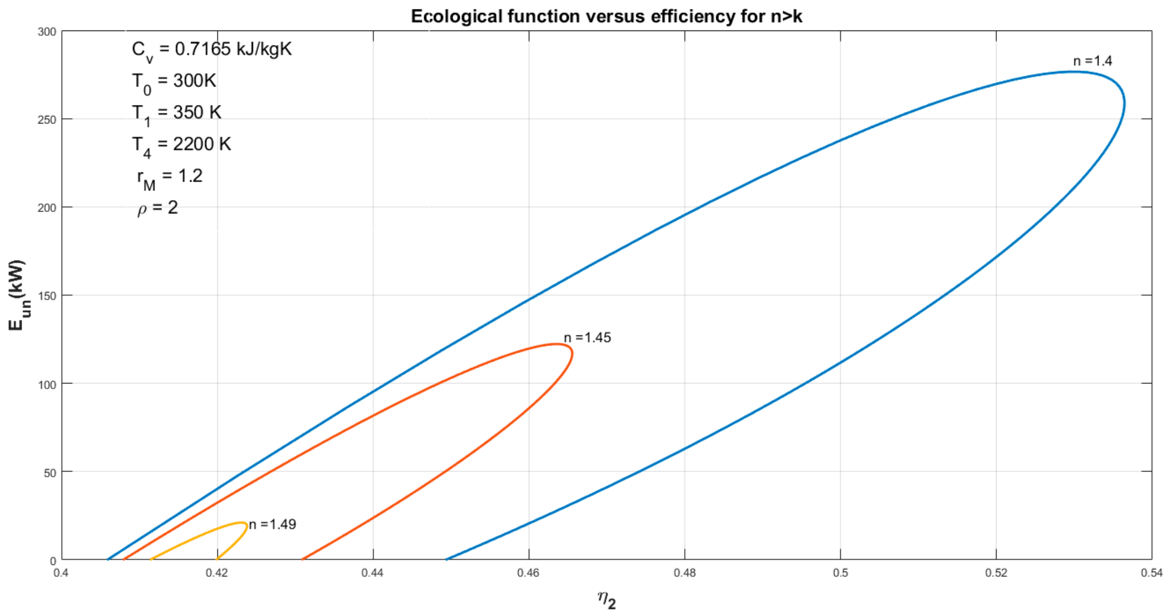

(**b**)

Figure 8. Impact of n ($n > k$) on E_{un}–P_2 (**a**) and E_{un}–η_2 (**b**).

As shown in Figure 9a. As the compression ratio increases, with a very steep gradient, the ECOP first increases to its maximum point and then begins to decrease. In addition, in a constant compression, then ECOP decreases with the increase of the n ($n > k$). Figure 9b,c shows that the maximum value of the coefficient of performance for various n ($n > k$) will occur at almost the maximum power and maximum thermal efficiency.

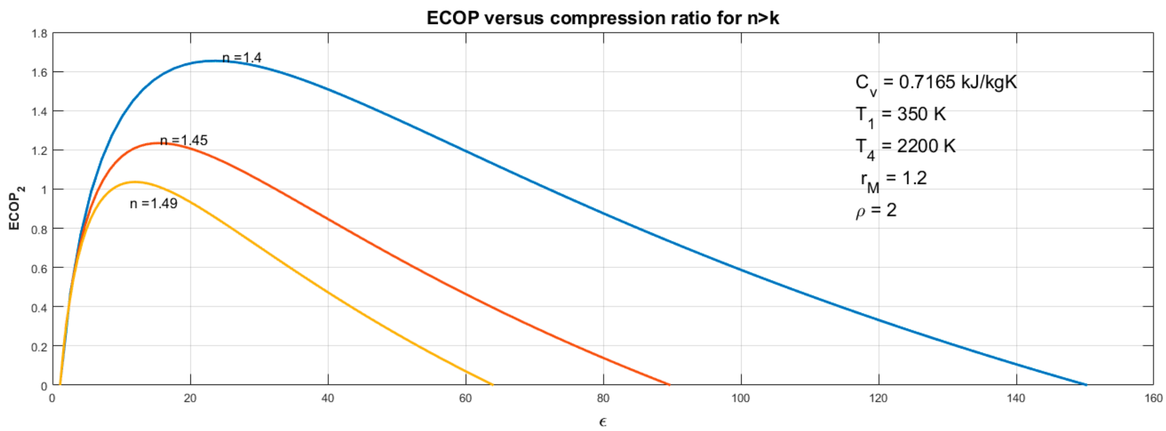

(**a**)

Figure 9. *Cont.*

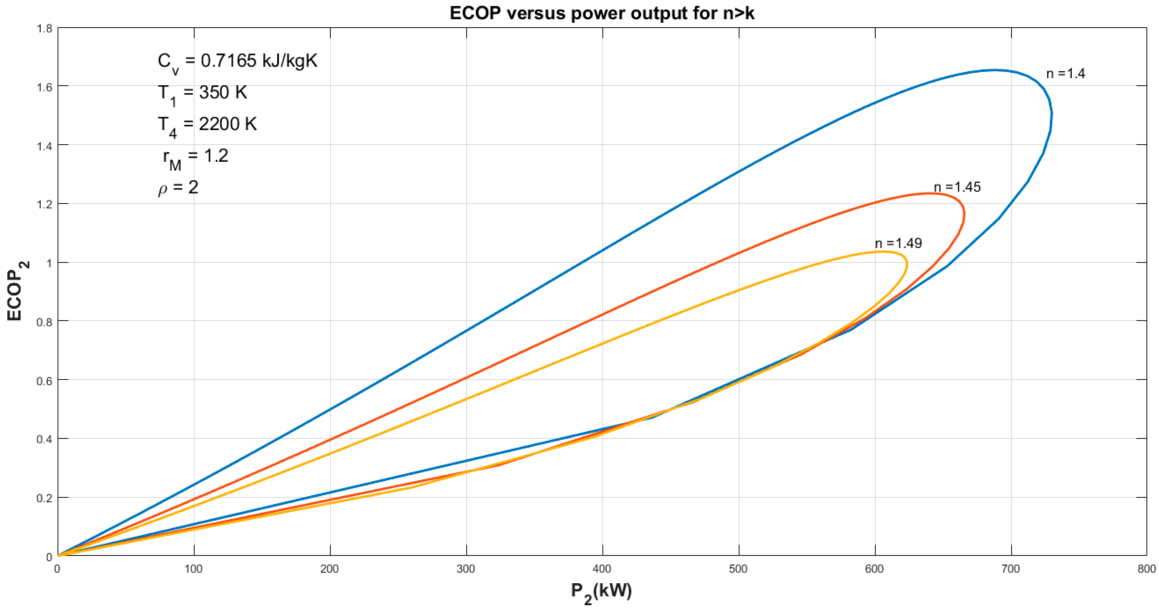

(**b**)

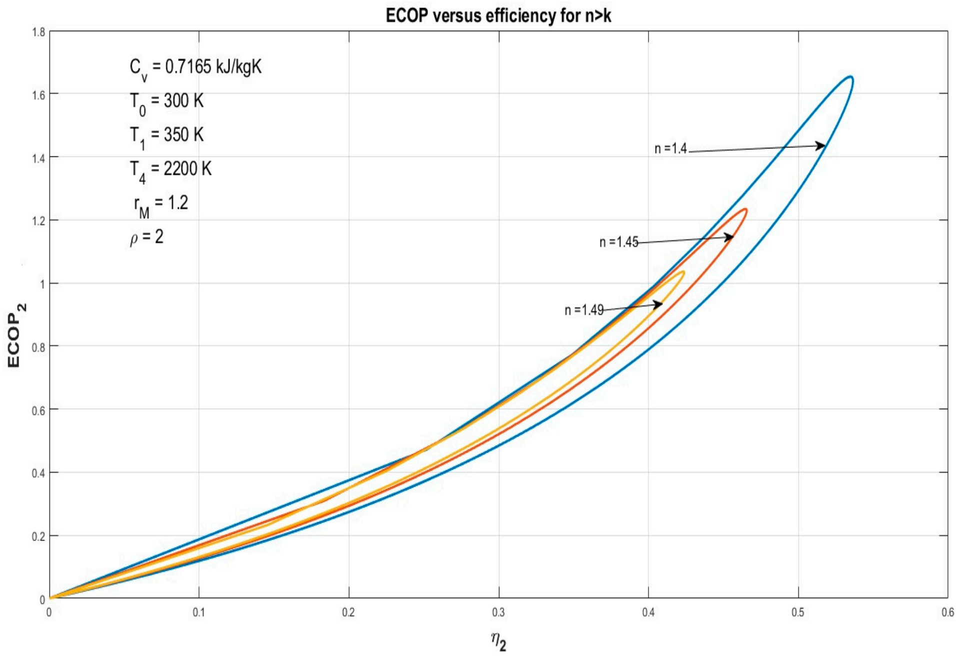

(**c**)

Figure 9. Effect of n ($n > k$) on ECOP−ε (**a**), ECOP–P_2 (**b**) and ECOP–η_2 (**c**).

4.3. Optimization Results for n Less than the k

Three objective functions are utilized in this optimization: η_1, ECOP and E_{un1}, described by Equations (26), (30) and (31), respectively. Also, three decision variables are considered: ε, ρ and n.

Although the decision variables might be various in the optimizing plan, they typically need to be fitted in a sensible range. Thus, the objective functions are determined by the limits of decision variables:

$$18 \leq \varepsilon \leq 25 \tag{50}$$

$$1.5 \leq \rho \leq 1.8 \tag{51}$$

$$1.2 \leq n \leq 1.4 \tag{52}$$

In this study η_1, ECOP and E_{un1} of the dual Miller cycle are maximized concurrently employing MOO by the mean of the NSGA-II approach. The objective functions are illustrated by Equations (26), (30) and (31) and the limitations by Equations (50)–(52).

The decision parameters of optimization are as follows: ε, ρ and n. The Pareto optimal frontier of objective functions (the thermal efficiency, ECOP, and E_{un1}) is depicted in Figure 10. All the optimized solutions for three objective functions obtained by NSGA II depicted in Figure 10. Selected points with different decision-making methods are presented, as well.

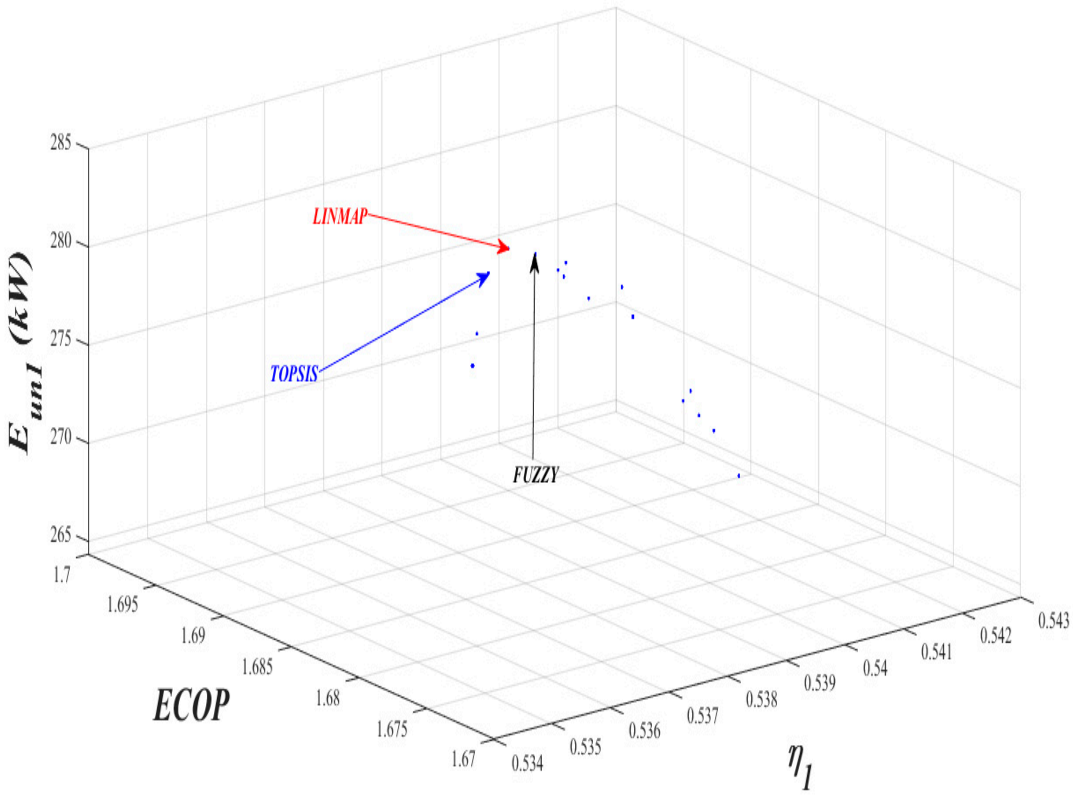

Figure 10. Distribution of the Pareto optimal frontier.

Table 1 outlines and compares the optimum values associated with the optimization elements utilizing Bellman-Zadeh, LINMAP, and TOPSIS approaches. In Table 1, the optimal solutions are determined for the considered objective functions and parameters used for decision by applying Fuzzy, LINMAP and TOPSIS methods and the outcomes of [102] for n less than k is represented. In order to calculate the results' deviation from the solutions in ideal and non-ideal conditions, Equations (53) to (55) are used.

$$d_+ = \sqrt{\left(\eta_1 - \eta_{1,n}\right)^2 + \left(E_{un1} - E_{un1,n}\right)^2 + \left(ECOP - ECOP_n\right)^2} \tag{53}$$

$$d_- = \sqrt{\left(\eta_1 - \eta_{1,n,non-ideal}\right)^2 + \left(E_{un1} - E_{un1,n,non-ideal}\right)^2 + \left(ECOP - ECOP_{n,non-ideal}\right)^2} \tag{54}$$

$$d = \frac{d_+}{(d_+) + (d_-)} \tag{55}$$

where $\eta_{1,n}$ refers to Euclidian the thermal efficiency, $E_{un1,n}$ is Ecological function and $ECOP_n$ denotes ECP. Moreover, in Table 1, the deviation index (d) of the data in each case is shown.

Table 1. Optimization results ($n < k$).

Optimization Method	Variables			Objective Functions			Deviation Index
	ε	ρ	n	η_1	ECOP	E_{un1}(kW)	
TOPSIS	19.4528	1.6852	1.4000	0.5373	1.6848	280.7994	0.0412
LINMAP	19.8660	1.6408	1.3999	0.5388	1.6899	279.2210	0.1333
Fuzzy	20.0708	1.5424	1.4000	0.54067	1.6959	275.5724	0.3462
[102] For maximum of η_1	27.8400	2.0000	1.4000	0.5364	1.3430	258.7400	0.8015
[102] For maximum of ECOP	15.7800	2.0000	1.4000	0.5174	1.6540	266.6000	0.8698
[102] For maximum of E_{un1}(kW)	19.8000	2.0000	1.4000	0.5300	1.6000	276.5300	0.2904
Ideal Solution	-	-	-	0.5428	1.6962	281.5052	0
Non-Ideal Solution	-	-	-	0.5346	1.6739	264.3691	∞

As represented in Table 1, in the cases of employing LINMAP, TOPSIS, and Fuzzy, the deviation indexes are 0.1333, 0.0412 and 0.3462, respectively. Based on these obtained values for deviation, it is concluded that employing TOSPSIS results in a more appropriate solution, therefore, the final solution is selected according to this method of decision making.

Table 2 demonstrates the comparative analysis of the optimization, utilizing the maximum absolute percentage error (MAAE) (see the first row), and the mean absolute percentage error (MAPE) (see the first row) to calculate the performance of the aforementioned optimization. Every optimization is run 30 times in MATLAB ® (9.5, MathWorks, Natick, MA, USA) software to deliver the ultimate results considering FUZZY Bellman-Zadeh, LINMAP, and TOPSIS methods.

Table 2. Comparative analysis presenting mean absolute percentage error (MAPE) and maximum absolute percentage error (MAAE).

Optimization Method	LINMAP			TOPSIS			Fuzzy		
Objectives	η_1	ECOP	E_{un1}(kW)	η_1	ECOP	$E_{un,1}$(kW)	η_1	ECOP	$E_{un,1}$(kW)
Max Error %	1.3610	1.4930	1.1620	1.2620	1.3840	1.2710	1.1830	1.6860	1.9430
Average Error %	0.5550	0.7340	0.4610	0.6340	0.6550	0.6020	0.4780	0.9360	0.8530

4.4. Optimization results for n higher than the k

Three objective functions are utilized in this optimization: η_2, ECOP and E_{un2}, described by Equations (44), (48) and (49), respectively. Also, three decision variables are considered: ε, ρ and n.

Although the decision variables might be different in the optimizing plan, they typically need to be fitted in a sensible range. Thus, the objective functions are determined by the limits of decision variables:

$$18 \leq \varepsilon \leq 25 \tag{56}$$

$$1.5 \leq \rho \leq 1.8 \tag{57}$$

$$1.4 < n \leq 1.6 \tag{58}$$

In this study, η_2, ECOP and E_{un2} of the dual Miller cycle are maximized concurrently utilizing MOO based on the NSGA-II approach. The objective functions are illustrated by Equations (48)–(50) and limitations by Equations (56)–(58).

The decision parameters of optimization are as follows: ε, ρ and n. The Pareto optimal frontier of objective functions (the thermal efficiency, ECOP, and E_{un2}) is depicted in Figure 11. All the optimized solutions for three objective functions obtained by NSGA II depicted in Figure 11. Selected points with different decision-making methods are presented, as well.

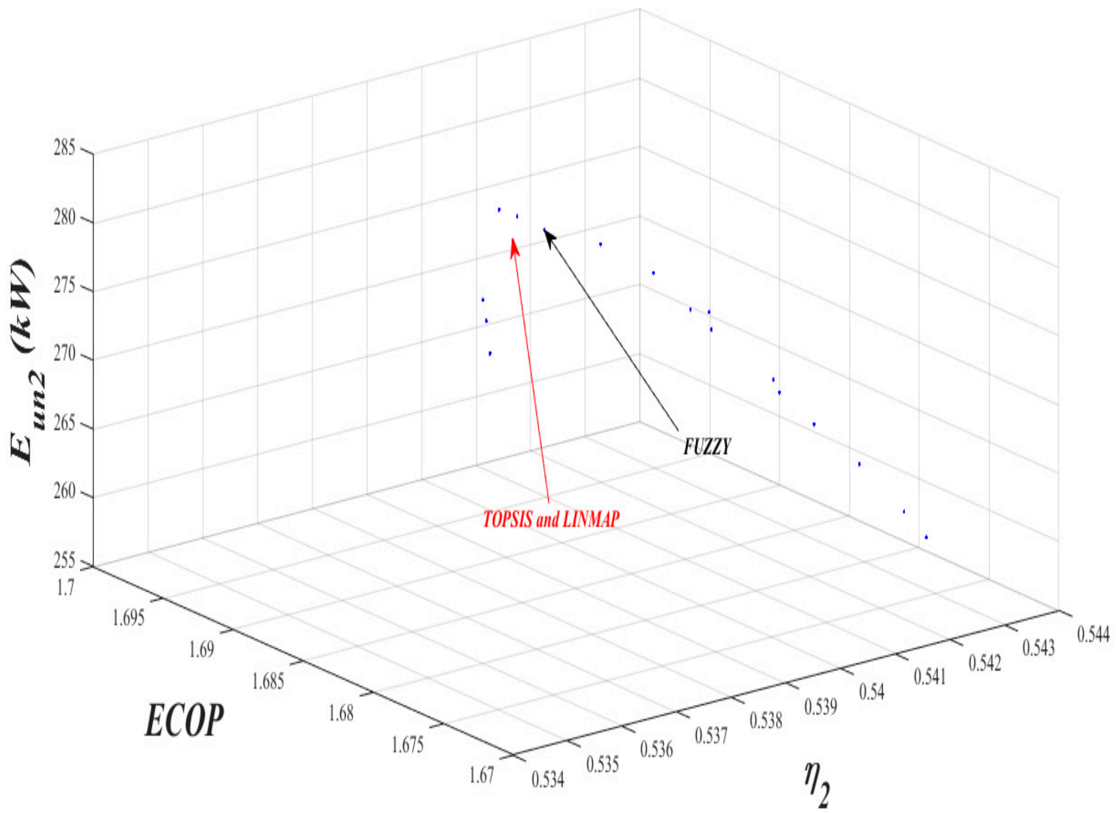

Figure 11. Distribution of the Pareto optimal frontier.

Table 3 outlines and compares the optimum values associated with the optimization elements utilizing Bellman-Zadeh, LINMAP, and TOPSIS approaches. In Table 3, the optimal answers to the objective functions and the employed variables for decision making are represented for the executed methods. In order to calculate the deviation from ideal and non-ideal cases, Equations (59) to (61) are used.

$$d_+ = \sqrt{\left(\eta_2 - \eta_{2,n}\right)^2 + (E_{un2} - E_{un2,n})^2 + (\mathrm{ECOP} - \mathrm{ECOP}_n)^2} \tag{59}$$

$$d_- = \sqrt{\left(\eta_2 - \eta_{2,n,non-ideal}\right)^2 + \left(E_{un2} - E_{un2,n,non-ideal}\right)^2 + \left(\mathrm{ECOP} - \mathrm{ECOP}_{n,non-ideal}\right)^2} \tag{60}$$

$$d = \frac{d_+}{(d_+) + (d_-)} \tag{61}$$

$\eta_{2,n}$ is Euclidian the thermal efficiency, $E_{un2,n}$ denotes Ecological function and ECOP_n refers to COP. In addition, the indexes of deviation in different considered cases are represented in Table 3.

As shown in Table 3, the indexes of deviation in the cases of employing Fuzzy, LINMAP and TOPSIS equal to 0.3173, 0.0696 and 0.0696, respectively. On the basis of the mentioned obtained values of deviation indexes, the final solution is selected by using LIMAP and TOPSIS for the dual Miller cycle.

Table 4 demonstrates the comparative analysis of the optimization, using MAAE and MAPE to calculate the performance of the aforementioned optimization. Every optimization is run 30 times in MATLAB ® software to deliver the ultimate results considering FUZZY Bellman-Zadeh, LINMAP, and TOPSIS methods.

Table 3. Optimization results ($n > k$).

Optimization Method	Variables			Objectives Functions			Deviation Index
	ε	ρ	n	η_2	ECOP	E_{un2}(kW)	
TOPSIS	20.2187	1.6870	1.4000	0.5385	1.6875	279.7315	0.0696
LINMAP	20.2187	1.6870	1.4000	0.5385	1.6875	279.7315	0.0696
Fuzzy	20.3829	1.5243	1.4000	0.5412	1.6959	273.7808	0.3173
[102] For maximum of η_1	27.8400	2.0000	1.4000	0.5364	1.3430	258.7400	0.9417
[102] For maximum of ECOP	15.7800	2.0000	1.4000	0.5174	1.6540	266.6000	0.6161
[102] For maximum of E_{un2}(kW)	19.8000	2.0000	1.4000	0.5300	1.6000	276.5300	0.2029
Ideal Solution	-	-	-	0.5435	1.6959	281.4043	0
Non-Ideal Solution	-	-	-	0.5347	1.6745	257.3777	∞

Table 4. Comparative analysis presenting MAPE and MAAE.

Optimization Method	LINMAP			TOPSIS			Fuzzy		
Objectives	η_2	ECOP	E_{un2}(kW)	η_2	ECOP	E_{un2}(kW)	η_2	ECOP	E_{un2}(kW)
Max Error %	0.8130	2.0580	2.0640	0.8130	1.2340	2.2604	1.1273	1.7732	2.9402
Average Error %	0.5421	0.8870	0.9210	0.5052	0.6450	0.9731	0.5690	0.9531	1.3503

5. Conclusions

A thermodynamic optimization has been carried out to obtain the thermal efficiency, ECOP, and E_{un} of the Dual-Miller Cycle. The compression ratio, the cut-off ratio, and the polytropic index are examined by the NSGA-II approach. Employing various decision-making methods (LINMAP, TOPSIS and fuzzy), the best optimum answer selected from the Pareto frontier. The study achieved a promising and satisfactory state of operation for Dual-Miller systems. The three methods give closed results (with a relative difference less than 3% on the compression ratio, 5% on cut-off ratio, 2% on the objective function. Two scenarios for optimization presented in this article that for the results of condition that ($n < k$) the best point has been LINMAP answer. The thermal efficiency for this point has been 0.5388. Also, the Ecological Coefficient of performance and Ecological function have been 1.6899 and 279.2210, respectively. For the results of the condition that ($n > k$) the best point has been LINMAP and TOPSIS answer. The thermal efficiency for this point has been 0.5385. Also, the Ecological Coefficient of performance and Ecological function have been 1.6875 and 279.7315, respectively. Finally, with the purpose of error investigation, average and maximum errors of obtained results are computed for every two scenarios. The results may be applicable to optimize the performance of practical Dual-Miller Cycle engines. The work which represents a theoretical investigation will be extended to an experimental investigation for future studies.

Author Contributions: Conceptualization, S.A., M.H.A. and S.M.P.; methodology, S.A., M.H.A. and S.M.P.; software, A.M., M.F.; validation S.A., M.H.A., S.M.P., F.P., A.M. and M.F.; formal analysis, S.A., M.H.A. and S.M.P.; investigation, S.A., M.H.A. and S.M.P.; resources, S.M.P., F.P., A.M., M.F. and S.S.; data curation, S.A., M.H.A., S.M.P. and F.P.; writing—original draft preparation, S.A., M.H.A., S.M.P. and F.P.; writing—review and editing, A.M.; visualization, S.A., M.H.A., S.M.P. and F.P.; supervision, M.H.A. and S.S.; project administration, M.F. and S.S.; funding acquisition, S.S.

Funding: This research received no external funding.

Conflicts of Interest: The authors declare no conflict of interest.

Nomenclature

DMC	Dual-Miller cycle
m	Mass flow rate (kg/S)
n	Polytropic exponent
k	The specific heat ratio (adiabatic exponent)
P	Power (kW)
Q	Heat (kW)
T	Temperature (K)
ECOP	Ecological Coefficient of Performance
E_{un}	Ecological function
V	volume
C_v	The specific heat at constant volume (kJ/kg.K)
C_p	The specific heat at constant pressure (kJ/kg.K)
σ_{un}	total entropy generation (kW/K)
η	Efficiency
r_M	The Miller cycle ratio of a Dual-Miller cycle
ρ	The cut-off ratio
λ	The pressure ratio
ε	The compression ratio
B	Heat transfer coefficient
T_0	Ambient temperature

References

1. Qin, Y.; He, Y.; Hiller, J.E.; Mei, G. A new water-retaining paver block for reducing runoff and cooling pavement. *J. Clean. Prod.* **2018**, *199*, 948–956. [CrossRef]
2. Qin, Y.; Zhang, M.; Hiller, J.E. Theoretical and experimental studies on the daily accumulative heat gain from cool roofs. *Energy* **2017**, *129*, 138–147. [CrossRef]
3. Qin, Y. Urban canyon albedo and its implication on the use of reflective cool pavements. *Energy Build.* **2015**, *96*, 86–94. [CrossRef]
4. Qin, Y.; Zhang, J.; Zheng, B.; Ma, X. Experimental study for the compressible behavior of warm and ice-rich frozen soil under the embankment of Qinghai–Tibet Railroad. *Cold Reg. Sci. Technol.* **2009**, *57*, 148–153. [CrossRef]
5. Curto-Risso, P.L.; Medina, A.; Calvo Hernández, A. Optimizing the geometrical parameters of a spark ignition engine: Simulation and theoretical tools. *Appl. Therm. Eng.* **2011**, *31*, 803–810. [CrossRef]
6. Curto-Risso, P.L.; Medina, A.; Hernández, A.C. Theoretical and simulated models for an irreversible Otto cycle. *J. Appl. Phys.* **2008**, *104*, 094911. [CrossRef]
7. Chen, L.G.; Wu, C.; Sun, F.R. Finite time thermodynamic optimization or entropy generation minimization of energy systems. *J. Non Equilib. Thermodyn.* **1999**, *24*, 327–359. [CrossRef]
8. Chen, L.G.; Sun, F.R. *Advances in Finite Time Thermodynamics: Analysis and Optimization*; Nova Science Publishers: New York, NY, USA, 2004.
9. Chen, L.G. *Finite Time Thermodynamic Analysis of Irreversible Process and Cycles*; Higher Education Press: Beijing, China, 2005.
10. Curto-Risso, P.L.; Medina, A.; Calvo Hernández, A. Optimizing the operation of a spark ignition engine: Simulation and theoretical tools. *J. Appl. Phys.* **2009**, *105*, 094904. [CrossRef]
11. Wu, F.; Chen, L.G.; Sun, F.R.; Yu, J. *Finite Time Thermodynamic Optimization of Stirling Machine*; Chemical Industry Press: Beijing, China, 2008. (In Chinese)
12. Andresen, B. *Finite-Time Thermodynamics*; Physics Laboratory II; University of Copenhagen: Copenhagen, Denmark, 1983.
13. Medina, A.; Curto-Risso, P.L.; Hernández, A.C.; Guzmán-Vargas, L.; Angulo-Brown, F.; Sen, A.K. Quasi-Dimensional Simulation of Spark Ignition Engines. In *Thermodynamic Optimization to Cyclic Variability*; Springer: London, UK, 2014.

14. Karami, M.; Farahani, S.D.; Kowsary, F.; Mosavi, A. Experimental Estimation of Temporal and Spatial Resolution of Coefficient of Heat Transfer in a Channel Using Inverse Heat Transfer Method. *arXiv preprint* **2019**, arXiv:1907.12376.
15. Hoffmann, K.H.; Andresen, B.; Salamon, P. Finite-time thermodynamics tools to analyze dissipative processes. In Proceedings of the 240 Conference: Science's Great Challences, Advances in Chemical Physics; Wiley: Hoboken, NJ, USA, 2014; Volume 157, pp. 57–67.
16. Ahmadi, M.H.; Ahmadi, M.A.; Sadatsakkak, S.A. Thermodynamic analysis and performance optimization of irreversible Carnot refrigerator by using multi-objective evolutionary algorithms (MOEAs). *Renew. Sustain. Energy Rev.* **2015**, *51*, 1055–1070. [CrossRef]
17. Chen, L.G.; Meng, F.K.; Sun, F.R. Thermodynamic analyses and optimization for thermoelectric devices: The state of the arts. *Sci. China Technol. Sci.* **2016**, *59*, 442–455. [CrossRef]
18. Chen, L.; Feng, H.; Xie, Z. Generalized thermodynamic optimization for iron and steel production processes: Theoretical exploration and application cases. *Entropy* **2016**, *18*, 353. [CrossRef]
19. Sieniutycz, S. *Thermodynamic Approaches in Engineering Systems*; Elsevier: Oxford, UK, 2016.
20. Chen, L.G.; Xia, S.J. *Generalized Thermodynamics Dynamic Optimization of Irreversible Processes*; Science Press: Beijing, China, 2016. (In Chinese)
21. Chen, L.G.; Xia, S.J. *Generalized Thermodynamics Dynamic Optimization of Irreversible Cycles*; Science Press: Beijing, China, 2016. (In Chinese)
22. Bi, Y.H.; Chen, L.G. *Finite Time Thermodynamic Optimization of Air Heat Pump Performance*; Science Press: Beijing, China, 2017. (In Chinese)
23. Ahmadi, M.H.; Ahmadi, M.A.; Pourfayaz, F. Thermal models for analysis of performance of Stirling engine: A review. *Renew. Sustain. Energy Rev.* **2017**, *68*, 168–184. [CrossRef]
24. Ge, Y.; Chen, L.; Sun, F. Progress in finite time thermodynamic studies for internal combustion engine cycles. *Entropy* **2016**, *18*, 139. [CrossRef]
25. Chen, L.; Zhang, W.; Sun, F. Power, efficiency, entropy-generation rate and ecological optimization for a class of generalized irreversible universal heat-engine cycles. *Appl. Energy* **2007**, *84*, 512–525. [CrossRef]
26. Zhou, B.; Cheng, X.T.; Liang, X.G. Power output analyses and optimizations of the Stirling cycle. *Sci. China Technol. Sci.* **2013**, *56*, 228–236. [CrossRef]
27. Ge, Y.; Chen, L.; Sun, F. Optimal path of piston motion of irreversible Otto cycle for minimum entropy generation with radiative heat transfer law. *J. Energy Inst.* **2012**, *85*, 140–149. [CrossRef]
28. Sun, F.; Chen, L.; Wang, C.; Xia, S. Optimal Concentration Configuration of Consecutive Chemical Reaction A ⇔ B ⇔ C for Minimum Entropy Generation. *J. Non Equilib. Thermodyn.* **2016**, *41*, 313–326.
29. Wu, Y.Q. Analyses of thermodynamic performance for the endoreversible Otto cycle with the concepts of entropy generation and entransy. *Sci. China Technol. Sci.* **2017**, *60*, 692–700. [CrossRef]
30. Angulo-Brown, F. An ecological optimization criterion for finite-time heat engines. *J. Appl. Phys.* **1991**, *69*, 7465–7469. [CrossRef]
31. Yan, Z.J. Comment on "ecological optimization criterion for finite time heat engines". *J. Appl. Phys.* **1993**, *73*, 3583. [CrossRef]
32. Angulo-Brown, F.; Fernández-Betanzos, J.; Diaz-Pico, C.A. Compression ratio of an optimized air standard Otto-cycle model. *Eur. J. Phys.* **1994**, *15*, 38–42. [CrossRef]
33. Chen, L.G.; Sun, F.R.; Chen, W.Z. The ecological quality factor for thermodynamic cycles (in Chinese). *J. Eng. Therm. Energy Power* **1994**, *9*, 374–376.
34. Long, R.; Li, B.; Liu, Z.; Liu, W. Ecological analysis of a thermally regenerative electrochemical cycle. *Energy* **2016**, *107*, 95–102. [CrossRef]
35. Üst, Y.; Sahin, B.; Kodal, A. Ecological coefficient of performance (ECOP) optimization for generalized irreversible Carnot heat engines. *J. Energy Inst.* **2005**, *78*, 145–151. [CrossRef]
36. Ust, Y.; Sahin, B.; Sogut, O.S. Performance analysis and optimization of an irreversible dual-cycle based on an ecological coefficient of performance criterion. *Appl. Energy* **2005**, *82*, 23–39. [CrossRef]
37. Ust, Y.; Sahin, B.; Kodal, A. Performance analysis of an irreversible Brayton heat engine based on ecological coefficient of performance criterion. *Int. J. Therm. Sci.* **2006**, *45*, 94–101. [CrossRef]
38. Ust, Y. Performance analysis and optimization of irreversible air refrigeration cycles based on ecological coefficient of performance criterion. *Appl. Therm. Eng.* **2009**, *29*, 47–55. [CrossRef]

39. Gonca, G.; Sahin, B. Performance optimization of an air-standard irreversible dual-Atkinson cycle engine based on the ecological coefficient of performance criterion. *Sci. World J.* **2014**, *2014*, 1–10. [CrossRef]
40. Ust, Y.; Sahin, B.; Cakir, M. Ecological coefficient of performance analysis and optimisation of gas turbines by using exergy analysis approach. *Int. J. Exergy* **2016**, *21*, 39–69. [CrossRef]
41. Salamon, P.; Hoffmann, K.H.; Schubert, S.; Berry, R.S.; Andresen, B. What conditions make minimum entropy production equivalent to maximum power production? *J. Non Equilib. Thermodyn.* **2001**, *26*, 73–83. [CrossRef]
42. Blank, D.A.; Wu, C. The effects of combustion on a power-optimized endoreversible Dual cycle. *Energy Conv. Manag.* **1994**, *14*, 98–103.
43. Chen, L.; Sun, F.; Wu, C. Optimal performance of an irreversible dual cycle. *Appl. Energy* **2004**, *79*, 3–14. [CrossRef]
44. Ust, Y.; Sahin, B.; Kayadelen, H.K.; Gonca, G. Heat transfer effects on the performance of an air-standard irreversible dual cycle. *Int. J. Veh. Des.* **2013**, *63*, 102. [CrossRef]
45. Ghatak, A.; Chakraborty, S. Effect of external irreversibilities and variable thermal properties of working fluid on thermal performance of a Dual internal combustion engine cycle. *Strojnicky Casopsis J. Mech. Energy* **2007**, *58*, 1–12.
46. Wang, W.; Chen, L.; Sun, F.; Wu, C. The effect of friction on the performance of an air standard dual cycle. *Exergy Int. J.* **2002**, *2*, 340–344. [CrossRef]
47. Ge, Y.; Chen, L.; Sun, F. Finite-time thermodynamic modeling and analysis for an irreversible Dual cycle. *Math. Comput. Model.* **2009**, *50*, 101–108. [CrossRef]
48. Al-Sarkhi, A.; Akash, B.; Jaber, J.; Mohsen, M.; Abu-Nada, E.; Akash, B. Efficiency of Miller engine at maximum power density. *Int. Commun. Heat Mass Transf.* **2002**, *29*, 1159–1167. [CrossRef]
49. Chen, L.; Ge, Y.; Sun, F.; Wu, C. The performance of a Miller cycle with heat transfer, friction and variable specific heats of working fluid. *Termotehnica* **2010**, *14*, 24–32.
50. Chen, L.; Ge, Y.; Sun, F.; Wu, C. Finite-time thermodynamic modelling and analysis for an irreversible Miller cycle. *Int. J. Ambient Energy* **2011**, *32*, 87–94. [CrossRef]
51. Lin, J.; Xu, Z.; Chang, S.; Yan, H. Finite-time thermodynamic modeling and analysis of an irreversible Miller cycle working on a four-stroke engine. *Int. Commun. Heat Mass Transf.* **2014**, *54*, 54–59. [CrossRef]
52. Gonca, G.; Sahin, B.; Ust, Y.; Parlak, A.; Safa, A. Comparison of steam injected diesel engine and Miller cycled diesel engine by using two zone combustion model. *J. Energy Inst.* **2015**, *88*, 43–52. [CrossRef]
53. Gonca, G.; Sahin, B.; Parlak, A.; Ust, Y.; Ayhan, V.; Cesur, I.; Boru, B. Theoretical and experimental investigation of the Miller cycle diesel engine in terms of performance and emission parameters. *Appl. Energy* **2015**, *138*, 11–20. [CrossRef]
54. Ebrahimi, R. Second law analysis on an air-standard miller engine. *Acta Phys. Pol. A* **2016**, *129*, 1079–1082. [CrossRef]
55. Mousapour, A.; Hajipour, A.; Rashidi, M.M.; Freidoonimehr, N. Performance evaluation of an irreversible Miller cycle comparing FTT (finite-time thermodynamics) analysis and ANN (artificial neural network) prediction. *Energy* **2016**, *94*, 100–109. [CrossRef]
56. Zhao, J. Research and application of over-expansion cycle (Atkinson and Miller) engines—A review. *Appl. Energ.* **2017**, *185*, 300–319. [CrossRef]
57. Gonca, G.; Sahin, B.; Ust, Y. Performance maps for an air-standard irreversible Dual-Miller cycle (DMC) with late inlet valve closing (LIVC) version. *Energy* **2013**, *54*, 285–290. [CrossRef]
58. Gonca, G.; Sahin, B.; Ust, Y. Investigation of heat transfer influences on performance of air-standard irreversible Dual-Miller cycle. *J. Thermophys. Heat Transf.* **2015**, *29*, 678–683. [CrossRef]
59. Gonca, G. Comparative performance analyses of irreversible OMCE (Otto Miller cycle engine)-DiMCE (Diesel miller cycle engine)-DMCE (Dual Miller cycle engine). *Energy* **2016**, *109*, 152–159. [CrossRef]
60. Ust, Y.; Arslan, F.; Ozsari, I.; Cakir, M. Thermodynamic performance analysis and optimization of DMC (Dual Miller Cycle) cogeneration system by considering exergetic performance coefficient and total exergy output criteria. *Energy* **2015**, *90*, 552–559. [CrossRef]
61. Gonca, G. Thermo-ecological analysis of irreversible Dual-Miller Cycle (DMC) engine based on the ecological coefficient of performance (ECOP) criterion. *Iran. J. Sci. Technol. Trans. Mech. Eng.* **2016**, *41*, 269–280. [CrossRef]
62. Gonca, G.; Sahin, B. Thermo-ecological performance analyses and optimizations of irreversible gas cycle engines. *Appl. Therm. Eng.* **2016**, *105*, 566–576. [CrossRef]

63. Wu, Z.X.; Chen, L.G.; Ge, Y.L.; Sun, F.R. Ecological objective function optimization of an irreversible Dual-Miller cycle with linear variable specific heat ratio of the working fluid (in Chinese). *Energy Conserv.* **2016**, *6*, 20–27.
64. Wu, Z.; Chen, L.; Ge, Y.; Sun, F. Power, efficiency, ecological function and ecological coefficient of performance of an irreversible Dual-Miller cycle (DMC) with nonlinear variable specific heat ratio of working fluid. *Eur. Phys. J. Plus* **2017**, *132*, 209. [CrossRef]
65. Huleihil, M.; Mazor, G. Irreversible performance characteristics of air standard Otto cycles with polytropic processes. *Appl. Mech. Eng.* **2012**, *1*, 1000111. [CrossRef]
66. Gong, S.W.; Chen, L.G.; Sun, F.R. Performance analysis and optimization of endoreversible Lenoir cycle with polytropic process (in Chinese). *Energy Conserv.* **2013**, *32*, 22–26.
67. Xiong, B.; Chen, L.G.; Ge, Y.L. Finite-time thermodynamic analysis of an endoreversible Otto cycle with polytropic process (in Chinese). *Power Energy* **2014**, *35*, 166–171.
68. Najafi, B.; Faizollahzadeh Ardabili, S.; Mosavi, A.; Shamshirband, S.; Rabczuk, T. An intelligent artificial neural network-response surface methodology method for accessing the optimum biodiesel and diesel fuel blending conditions in a diesel engine from the viewpoint of exergy and energy analysis. *Energies* **2018**, *11*, 860. [CrossRef]
69. Özyer, T.; Zhang, M.; Alhajj, R. Integrating multi-objective genetic algorithm based clustering and data partitioning for skyline computation. *Appl. Intell.* **2011**, *35*, 110–122. [CrossRef]
70. Beatrice, O.; Brian, J.R.; Franklin, H. Multi-Objective Genetic Algorithms for Vehicle Routing Problem with Time Windows. *Appl. Intell.* **2006**, *24*, 17–30.
71. Blecic, I.; Cecchini, A.; Trunfio, G. A decision support tool coupling a causal model and a multi-objective genetic algorithm. *Appl. Intell.* **2007**, *26*, 125–137. [CrossRef]
72. Veldhuizen, D.A.V.; Lamont, G.B. *Multi Objective Evolutionary Algorithms Analyzing the State-of-the-Art*; MIT Press: Cambridge, MA, USA, 2000.
73. Konak, A.; Coit, D.W.; Smith, A.E. Multi-objective optimization using genetic algorithms: A tutorial. *Reliab. Eng. Syst. Saf.* **2006**, *91*, 992–1007. [CrossRef]
74. Ahmadi, M.H.; Hosseinzade, H.; Sayyaadi, H.; Mohammadi, A.H.; Kimiaghalam, F. Application of the multi-objective optimization method for designing a powered Stirling heat engine: Design with maximized power, thermal efficiency and minimized pressure loss. *Renew. Energy* **2013**, *60*, 313–322. [CrossRef]
75. Ahmadi, M.H.; Sayyaadi, H.; Mohammadi, A.H.; Barranco-Jimenez, M.A. Thermo-economic multi-objective optimization of solar dish-Stirling engine by implementing evolutionary algorithm. *Energy Convers. Manag.* **2013**, *73*, 370–380. [CrossRef]
76. Ahmadi, M.H.; Sayyaadi, H.; Dehghani, S.; Hosseinzade, H. Designing a solar powered Stirling heat engine based on multiple criteria: Maximized thermal efficiency and power. *Energy Convers. Manag.* **2013**, *75*, 282–291. [CrossRef]
77. Ahmadi, M.H.; Dehghani, S.; Mohammadi, A.H.; Feidt, M.; Barranco-Jimenez, M.A. Optimal design of a solar driven heat engine based on thermal and thermo-economic criteria. *Energy Convers. Manag.* **2013**, *75*, 635–642. [CrossRef]
78. Cui, T.; Zhao, W.; Wang, C. Design Optimization of Vehicle EHPS System Based on Multi-objective Genetic Algorithm. *DEStech Trans. Environ. Energy Earth Sci.* **2019**, *179*, 100–110.
79. Lazzaretto, A.; Toffolo, A. Energy, economy and environment as objectives in multi-criterion optimization of thermal systems design. *Energy* **2004**, *29*, 1139–1157. [CrossRef]
80. Ahmadi, M.H.; Mohammadi, A.H.; Pourkiaei, S.M. Optimisation of the thermodynamic performance of the Stirling engine. *Int. J. Ambient. Energy* **2014**, *37*, 1–13. [CrossRef]
81. Toffolo, A. Evolutionary algorithms for multi-objective energetic and economic optimization in thermal system design. *Energy* **2002**, *27*, 549–567. [CrossRef]
82. Ahmadi, M.H.; Mohammadi, A.H.; Dehghani, S. Evaluation of the maximized power of a regenerative endoreversible Stirling cycle using the thermodynamic analysis. *Energy Convers. Manag.* **2013**, *76*, 561–570. [CrossRef]
83. Ahmadi, M.H.; Ahmadi, M.A.; Feidt, M. Performance Optimization of a Solar-Driven Multi-Step Irreversible Brayton Cycle Based on a Multi-Objective Genetic Algorithm. *Oil Gas Sci. Technol. Rev. IFP Energies Nouv.* **2014**, *71*, 16. [CrossRef]

84. Arora, R.; Kaushik, S.; Arora, R. Multi-objective and multi-parameter optimization of two-stage thermoelectric generator in electrically series and parallel configurations through NSGA-II. *Energy* **2015**, *91*, 242–254. [CrossRef]
85. Ahmadi, M.H.; Ahmadi, M.A. Thermodynamic analysis and optimization of an irreversible Ericsson cryogenic refrigerator cycle. *Energy Convers. Manag.* **2015**, *89*, 147–155. [CrossRef]
86. Ahmadi, M.H.; Ahmadi, M.A. Thermodynamic analysis and optimisation of an irreversible radiative-type heat engine by using non-dominated sorting genetic algorithm. *Int. J. Ambient. Energy* **2014**, *37*, 1–6. [CrossRef]
87. Ahmadi, M.H.; Ahmadi, M.A.; Mehrpooya, M.; Sameti, M. Thermo-ecological analysis and optimization performance of an irreversible three-heat-source absorption heat pump. *Energy Convers. Manag.* **2015**, *90*, 175–183. [CrossRef]
88. Mahmoudimehr, J.; Sebghati, P. A novel multi-objective Dynamic Programming optimization method: Performance management of a solar thermal power plant as a case study. *Energy* **2019**, *168*, 796–814. [CrossRef]
89. Ahmadi, M.H.; Jokar, M.A.; Ming, T.; Feidt, M.; Pourfayaz, F.; Astaraei, F.R. Multi-objective performance optimization of irreversible molten carbonate fuel cell–Braysson heat engine and thermodynamic analysis with ecological objective approach. *Energy* **2018**, *144*, 707–722. [CrossRef]
90. Jokar, M.A.; Ahmadi, M.H.; Sharifpur, M.; Meyer, J.P.; Pourfayaz, F.; Ming, T. Thermodynamic evaluation and multi-objective optimization of molten carbonate fuel cell-supercritical CO 2 Brayton cycle hybrid system. *Energy Convers. Manag.* **2017**, *153*, 538–556. [CrossRef]
91. Li, J.-Q.; Sang, H.-Y.; Han, Y.-Y.; Wang, C.-G.; Gao, K.-Z. Efficient multi-objective optimization algorithm for hybrid flow shop scheduling problems with setup energy consumptions. *J. Clean. Prod.* **2018**, *181*, 584–598. [CrossRef]
92. Ahmadi, M.H.; Ahmadi, M.-A.; Maleki, A.; Pourfayaz, F.; Bidi, M.; Açıkkalp, E. Exergetic sustainability evaluation and multi-objective optimization of performance of an irreversible nanoscale Stirling refrigeration cycle operating with Maxwell–Boltzmann gas. *Renew. Sustain. Energy Rev.* **2017**, *78*, 80–92. [CrossRef]
93. Xu, F.; Liu, J.; Lin, S.; Dai, Q.; Li, C. A multi-objective optimization model of hybrid energy storage system for non-grid-connected wind power: A case study in China. *Energy* **2018**, *163*, 585–603. [CrossRef]
94. Ahmadi, M.H.; Ahmadi, M.A. Multi objective optimization of performance of three-heat-source irreversible refrigerators based algorithm NSGAII. *Renew. Sustain. Energy Rev.* **2016**, *60*, 784–794. [CrossRef]
95. Ahmadi, M.H.; Ahmadi, M.A.; Pourfayaz, F. Thermodynamic analysis and evolutionary algorithm based on multi-objective optimization performance of actual power generating thermal cycles. *Appl. Therm. Eng.* **2016**, *99*, 996–1005. [CrossRef]
96. Niu, X.; Wang, H.; Hu, S.; Yang, C.; Wang, Y. Multi-objective online optimization of a marine diesel engine using NSGA-II coupled with enhancing trained support vector machine. *Appl. Therm. Eng.* **2018**, *137*, 218–227. [CrossRef]
97. Deb, M.; Debbarma, B.; Majumder, A.; Banerjee, R. Performance –emission optimization of a diesel-hydrogen dual fuel operation: A NSGA II coupled TOPSIS MADM approach. *Energy* **2016**, *117*, 281–290. [CrossRef]
98. Ahmadi, M.H.; Ahmadi, M.A.; Mellit, A.; Pourfayaz, F.; Feidt, M. Thermodynamic analysis and multi objective optimization of performance of solar dish Stirling engine by the centrality of entransy and entropy generation. *Int. J. Electr. Power Energy Syst.* **2016**, *78*, 88–95. [CrossRef]
99. Wang, J.; Duan, L.; Yang, Y.; Pang, L.; Yang, L. Multi-objective optimization of solar-aided coal-fired power generation system under off-design work conditions. *Energy Sci. Eng.* **2019**, *7*, 379–398. [CrossRef]
100. Wang, S.; Wang, K.; Teng, F.; Strbac, G.; Wu, L. An affine arithmetic-based multi-objective optimization method for energy storage systems operating in active distribution networks with uncertainties. *Appl. Energy* **2018**, *223*, 215–228. [CrossRef]
101. Tian, W.; Jiang, C.; Ni, B.; Wu, Z.; Wang, Q.; Yang, L. Global sensitivity analysis and multi-objective optimization design of temperature field of sinter cooler based on energy value. *Appl. Therm. Eng.* **2018**, *143*, 759–766. [CrossRef]
102. Jiang, Y.; Chen, L.; Wu, Z.; Sun, F. Thermodynamic performance of Dual-Miller cycle (DMC) with polytropic processes based on power output, thermal efficiency and ecological function. *Sci. China Technol. Sci.* **2018**, *61*, 453–463.

103. Klein, S.A. An explanation for observed compression ratios in internal combustion engines. *J. Eng. Gas Turbines Power* **1991**, *113*, 511–513. [CrossRef]
104. Mosavi, A. Application of multi-objective optimization packages in design of an evaporator coil. *World Acad. Sci. Eng. Technol.* **2010**, *61*, 25–29.
105. Zhang, S.; Karimi, S.; Shamshirband, S.; Mosavi, A. Optimization Algorithm for Reduction the Size of Dixon Resultant Matrix: A Case Study on Mechanical Application. *Comput. Mater. Contin.* **2019**, *58*, 567–583. [CrossRef]
106. Mosavi, A.; Rabczuk, T. Learning and Intelligent Optimization for Material Design Innovation. Learning and Intelligent Optimization. In *Lecture Notes in Computer Science*; Springer: Cham, Switzerland, 2017; Volume 10556, pp. 120–139.
107. Mosavi, A.; Rituraj, R.; Varkonyi-Koczy, A.R. Review on the Usage of the Multiobjective Optimization Package of modeFrontier in the Energy Sector. *Adv. Intell. Syst. Comput.* **2018**, *660*, 217–224.
108. Ge, Y.; Chen, L.; Sun, F. Ecological optimization of an irreversible Otto cycle. *Arab. J. Sci. Eng.* **2013**, *38*, 373–381. [CrossRef]
109. Ge, Y.; Chen, L.; Sun, F.; Wu, C. Effects of heat transfer and variable specific heats of working fluid on performance of a Miller cycle. *Int. J. Ambient Energy* **2005**, *26*, 203–214. [CrossRef]
110. Qin, Y.; Hiller, J.E.; Bao, T. Modeling Cold Region Ground Temperatures with a Heat Flux Upper Boundary Model. *J. Cold Reg. Eng.* **2013**, *27*, 29–43. [CrossRef]
111. Qin, Y.; Hiller, J.E. Understanding pavement-surface energy balance and its implications on cool pavement development. *Energy Build.* **2014**, *85*, 389–399. [CrossRef]
112. Qin, Y. A review on the development of cool pavements to mitigate urban heat island effect. *Renew. Sustain. Energy Rev.* **2015**, *52*, 445–459. [CrossRef]